Role of electron-electron interactions in electron emission from nanotube materials

Naira Grigoryan [1] and Piotr Chudzinski [1,2]

[1] *Institute of Fundamental Technological Research, Polish Academy of Sciences, Adolfa Pawińskiego 5b, 02-106 Warsaw, Poland*

[2] *School of Mathematics and Physics, Queen's University Belfast, University Road, Belfast, BT7 1NN Northern Ireland, United Kingdom*

(Received 18 August 2023; accepted 8 December 2023; published 29 January 2024)

Nanotubes and nanorods have been recently established as very good materials to work as electron sources in a field emission (FE) process. These are one-dimensional materials and electron-electron interactions are expected to play a crucial role in their physics. Here we study the influence of electron-electron interactions on the field emission. We study the problem in the low energy regime; thus we need to abandon the antiadiabatic approximation and derive tunneling amplitude for a finite duration of the tunneling process. In this work we identified the parameters when exact analytic expression for tunneling current can be given. We obtained formalism that enables one to capture *at the same time* the collective effects due to electron-electron interactions and thermionic emission. Our results reveal that different types of nanotubes, and their minigap/compressibility parameters, can be easily distinguished based on FE measurements on these materials.

DOI: 10.1103/PhysRevMaterials.8.016003

I. INTRODUCTION

Field emission (FE), a process of electron's tunneling through the barrier on materials' surface due to the presence of an external electric field, has several important applications, both technological and fundamental and remains a very active field of research [1]. From the technological point of view, it enables us to create stable electron beam sources, critical for electron microscopy [2,3] and vacuum electronics [4–6]. From the fundamental point of view, it enables one to diagnose a microstructure of the material in question. It is then no surprise that many decades of research have been dedicated to developing the theory of this process [7]. The situation when the material can be described within a single particle framework has been largely captured [8]. In this case, presently, efforts are being focused on issues of how to describe best the local electric field [9–11] and how to merge the formalism with the *ab initio* methods that describe materials [12,13].

The situation is much less clear when interactions, and correlations, play a substantial role. The questions of how the electron-electron interactions affect the field emission, and also how they conspire with thermal effect to produce the total current in a real device, remained largely unanswered. Here we identify one class of materials—the arrays of nanotubes—where a fully analytic answer can be given to these questions.

Arrays of carbon nanotubes have been identified as a promising material for field emission, especially due to their large brightness already at low voltages [14], which is an important aspect from the point of view of safety and energy efficiency [15–17]. These structures constitute many one-dimensional (1D) systems that were grown in parallel from the substrate, as shown in Fig. 1. Interactions are crucial in 1D systems as the electrons in their motion cannot avoid each other. This has later led to a proposal of a new paradigm—a collective Tomonaga-Luttinger liquid (TLL), an alternative to canonical Landau-Fermi liquid—an achievement that was later experimentally confirmed and for which Haldane got a Nobel prize in physics. This collective nature of basic excitations affects all observables. The effect of field emission is no exception. Despite that, there have been only a few past studies of field emission within the TLL framework and they focused on a zero-temperature, infinitely long 1D system that is suspended flat on the top of a surface [18,19]. This is quite different geometry than in the devices of currently common interest. Two developments of the theory are necessary to achieve the aim of bringing theoretical description closer to the experimental setting. First, for a low energy field emission the tunneling process cannot be considered as instantaneous, so we need to abandon the antiadiabatic approximation and consider the dynamics of the tunneling at least in a saddle point approximation. Secondly, we need to abandon the assumption of translational invariance—in order to explore varying probabilities of tunneling along the nanotube we need to derive the local density of states along the nanotube. Both of these developments are achieved in this work.

So far a grand majority of works dedicated to field emission from nanotubes and nanotubes' arrays has focused on the area at the tip of the nanotube [10,20–22]. As explained above, this is because there is a hope that a single particle picture may provide the dominant contribution in such processes, which simplifies the theory substantially. There are very detailed studies of electrostatic potential in this area and an in-depth microscopic analysis on the single-particle picture, reaching a level of material specific DFT calculations [23]. The argument is that therein the electric field is the strongest. While we did

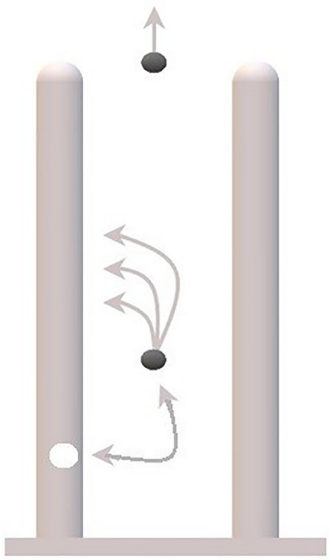

FIG. 1. Schematic illustration of the problem we consider here: an array of nanotubes that are vertically grown on the substrate. The electron (black dot) is emitted from the nanotube and during the propagation it still interacts with the hole inside of the nanotube (white spot).

not disregard this argument, we wish to focus here on the remaining side surface of the nanotube where the 1D collective effects will be the strongest. From the standard point of a well-studied single-particle emission from the nanotubes' tips this large emitting area will provide a so-called incoherent background and the two signals will add up, as experimentally shown in Ref. [1]. The importance of this side-area emission has been recognized both experimentally [24] and theoretically [25], but that theory did not include electron-electron interactions inside the nanotube. We shall obtain here exact analytical expressions for the strongly correlated case and show that this background is not just a small correction, quite the opposite of that, and moreover that it can provide valuable insight into many-body physics inside the nanotube.

The outline of the paper is as follows. In Sec. II we present the theoretical framework that we use to describe the 1D correlated metal (Sec. II A) (from which the emission takes place), the Tomonaga-Luttinger liquid, and the recently obtained generalization of the canonical Fowler-Nordheim (gFN) tunneling theory (Sec. II B). In Sec. III we describe how the gFN can be applied to our problem. In Sec. IV we present our results: first gFN with TLL parameters incorporated (Sec. IV A), then Fourier transforms of TLL local density of states (LDOS) (Sec. IV B), and then we bring the two together to obtain the tunneling current (Sec. IV C). In the following Sec. V we apply the method to the nanotubes problem, where we tackle both gapless nanotubes and nanotubes with minigaps. The work is concluded with a brief discussion of its relevance in Sec. VI.

II. MODEL

A. Collective 1D liquid

TLL is a low energy state of collective excitations that provides a highly nontrivial solution for a strongly correlated 1D system. While the fermionic system is strongly interacting, upon bosonization we arrive at the solvable theory. The fermionic field operators $\psi(x)$ are rewritten in terms of bosonic density $\phi(x)$ and momentum $\theta(x)$ fields:

$$\psi(x) = \exp \imath k_F x \, \exp \imath \left(\sum_{\nu}^{N} \phi_\nu(x) + \theta_\nu(x) \right) \Big/ \sqrt{N}, \quad (1)$$

where N is the number of bosonic fields in the model. The bosonized Hamiltonian of the TLL state, i.e., written in terms of fluctuations of these collective bosonic modes, is

$$H^{1D} = \sum_{\nu}^{N} \int \frac{dx}{2\pi} \left[(v_\nu K_\nu)(\pi \Pi_\nu)^2 + \left(\frac{v_\nu}{K_\nu} \right) (\partial_x \phi_\nu)^2 \right], \quad (2)$$

where $\nabla\phi_\nu(x)$ gives the local density of fluctuations, while v_ν and K_ν are respectively the velocity and the TLL parameter ($\sim$ compressibility) of a given bosonic mode ν that depend on electron-electron interactions with small momentum exchange. In the simplest approximation, we assume Galilean invariance, which implies $v_\nu K_\nu \approx v_F$, where v_F is a Fermi velocity which in turn is approximated by Λ, an energy scale associated with the UV cutoff of our theory ($\equiv$bandwidth for a single band material, but more generally Λ spans the energy range where dispersion is linear). When, as is the case for carbon nanotubes (CNT), the gapless states can be grouped into pairs existing in two valleys at K, K' points of the Brillouin zone (BZ), there are two bands crossing the Fermi level and a two-leg ladder description applies. Then there are four bosonic modes $\rho\pm$, $\sigma\pm$, corresponding to the spin and charge modes oscillating symmetrically or antisymmetrically within the two legs of the ladder and referred to as the total and transverse modes, respectively. The total mode is a density fluctuation occurring simultaneously in both legs (the valleys), while the transverse mode is a density fluctuation propagating in the opposite direction in two adjacent legs of the ladder.

The K_ν parameters, proportional to compressibilities of collective modes, incorporate all electron-electron interactions with small momentum exchange $W_{\text{Hart}}(q \to 0)$—the so-called Hartree interactions. This is particularly useful for materials such as CNTs with electron-electron Coulomb interactions, where $W(q) \sim 1/q$ such that $W_{\text{Hart}}(q \to 0)$ indeed dominates. Furthermore, if these interactions do not depend on spin and valley degrees of freedom, then only the parameters of the total charge mode $\rho+$ will be affected.

B. Tunneling barrier

The physics that we want to capture is that of an electron tunneling through a barrier described by a potential $V(x)$. The lowest order approach to this problem is within the Wentzel-Kramers-Brillouin (WKB) approximation. In the past studies, when any attempt for exact analytical expression was made, the $V(x)$ had been given by the following expression:

$$V_0(x) = h - eFx - \frac{e^2}{16\pi\epsilon_0 x}, \quad (3)$$

where $h = \omega_0 - \omega$ (ω_0 is the work function characteristic of the given material and ω is the energy), the first term is an unscreened external electric field, while the last term is an

interaction with an "image" hole left behind in a metal. This has led [26] to an expression for the tunneling probability in terms of elliptic integrals, which was later rewritten [27] as a solution of a hypergeometric equation, suggesting a possibility for further generalizations.

Looking for a description of a tunneling process from a correlated electron liquid, we turn to the recently obtained [28] generalization of this expression for the potential in the following form:

$$V(x) = h - e\tilde{t}_{\rm tun}F_{\rm eff}x^{\alpha} - \frac{e^2\mathcal{G}_{eh}}{16\pi\epsilon_0 x^{\alpha}}, \tag{4}$$

where we generalized the previous formula by admitting that the *driving* term is an arbitrary power law with a prefactor proportional to some effective tunneling times some effective electric field, while the *interaction* term with nanotubes is proportional to some electron-hole propagator $\mathcal{G}_{eh}$. The assumption is that the functional dependence, the power law, remains, which as we show below is indeed very likely for the TLL environment. When $\alpha \equiv 1$ Eq. (4) simplifies to the previously considered Eq. (3). In our recent work [28], we found that for the special case when the absolute value of powers in the last two terms is equal the expression for the tunneling probability can be expressed in a close analytic form, i.e., in terms of a hypergeometric function; see Eq. (7) below.

The transmission probability is in general equal to the element of the density matrix that corresponds to the system with an emitted carrier. This is equal to $\mathcal{T} = \rho_{\rm tun}/Z$, where Z is a partition function of the system for which we take $Z = \rho_0 + \rho_{\rm tun} \approx 1 + \rho_{\rm tun}$, where we assume that the tunneling process is so negligible that it does not affect the density matrix of the rest of the system. Since $\rho_{\rm tun} = \exp(-S_{\rm tun})$ and anticipating the result Eq. (8) we obtain that $\mathcal{T}$ is expressed by Kemble's improved Jeffreys-Wentzel-Kramers-Brillouin (JWKB) formula:

$$\mathcal{T}(F,\omega) = \frac{1}{1 + D(F, h = \omega - \omega_0)}, \tag{5}$$

where, including explicitly the elementary constants $e, m_e, \hbar_P$ (which we set to $= 1$ from now on),

$$D(F,h) = \exp\left[\left(\frac{m_e^{\frac{1}{2}}}{e\hbar_P}\right)\left(\frac{h^{\frac{3}{2}}}{F}\right)\left(\frac{h}{2eF}\right)^{\frac{1-\alpha}{\alpha}}\left(\frac{2^{1-\frac{1-\alpha}{\alpha}}}{\alpha}\right)I(F,h)\right] \tag{6}$$

and the WKB integral $I(F,h,x) = \int_{x\rm in}^{x\rm out}\sqrt{V(x)}$ reads

$$I(F,h,x) = \frac{\pi\alpha x^{\frac{1}{\alpha}-\frac{3}{2}}\left\{2\zeta x^2[(\alpha-1)\zeta+1]\,{}_2F_1\left(\frac{1}{2},\frac{3}{2}-\frac{1}{\alpha};1;1-\zeta\right) - \alpha(\zeta+1)x^2\,{}_2F_1\left(-\frac{1}{2},\frac{3}{2}-\frac{1}{\alpha};1;1-\zeta\right)\right\}}{(\alpha^2-4)}, \tag{7}$$

where $\zeta = m/n$, $m = (\sqrt{1-\frac{F}{(\omega_0-\omega)^2}}+1)^{1/\alpha}$, and $n = (1-\sqrt{1-\frac{F}{(\omega_0-\omega)^2}})^{1/\alpha}$.

We confirmed [28] that the expression above for $\alpha = 1$ simplifies the previously obtained result in terms of elliptic integrals [29,30] for single-particle case Eq. (3). Our aim in the following section will be to build the connection between the exponent α in the formula above and the correlation effects in the nanotube.

III. TUNNELING PROCESS

As we have an array of nanotubes, the escaping mode of the electron is confined and takes place in the quantum well that is created by neighboring nanotubes (Fig. 1).

We consider dense array of nanotubes. The dense array is defined as an array that supports quantum wells between nanotubes and thus perpendicular confinement of an emitted electron. They interact with each other through Coulomb interactions which creates narrow wells of potential in between them and can also affect the physics of the tubes. Fortunately, this last phenomenon can be captured by an appropriate modification of the TLL parameters; to be precise for Coulomb interactions this affects only the effective $K_{\rho+}$ parameter [31]. Thus we have a problem of deep wells of potential in between the tubes. Each tube is described by TLL with some effective $K_{\rho+}$ and one expects that emitted electrons propagate within these potential minima. The issue that we want to address here is a dynamics of an electron as it propagates *along* the nanotube and in the process still can interact with the TLL electrons inside the tube. The usual approximation is to compute a saddle point (quasiclassical) configuration of the fields for a tunneling event taking place in a negligibly short time—the instanton gas approximation. However, the situation in the nanotube array is different, as the tunneling electron has to travel all the way up towards the top of the nanotube, in the meantime experiencing the influence of TLL. To solve this complicated case we decided to separate quasiclassical and quantum degrees of freedom [32]: $S = S_{\rm clas}(q) + S_{\rm quant}(\psi)$, with the former ones describing the time extended tunneling process $S_{\rm clas}(q) \equiv S_{\rm tun}(q)$, where $q(\tau)$ is a trajectory of escaping the single electron which takes place in an effective, averaged potential determined by quantum fluctuations $S_{\rm quant} \equiv \sum S_{1D}$, where $\psi(x,t)$ are wave functions inside the nanotubes. In other words, the classical trajectory includes the averaged TLL effect, as encoded in its known correlation functions, in the potential experienced by the escaping carrier. This may be thought of as a vertex correction to the tunneling matrix (operator) elements, a quantity whose importance has been emphasized before [33], where it has been accessed using alternative diagrammatic methods.

Following the seminal result by Coleman [34], the Euler-Lagrange equation for the instanton gives classical equation of motion $\ddot{q} = V_{\rm saddle}[q(\tau)]$, which admits a tunneling type solution; upon inserting it into the tunneling action one finds

$$S_{\rm tun} = \int d\tau\sqrt{V_{\rm saddle}[q(\tau)]}, \tag{8}$$

where we expect that V_{saddle} will have the form of Eq. (4). Remarkably, for the simplest case of straightforward motion perpendicular to the barrier, this becomes equivalent to the quasiclassical WKB result; however, in more complicated cases, such as ours, it will follow the trajectory of a particle in a spirit similar to the path-integral formulation. Now the $q(\tau)$ is the saddle point trajectory and we assume that, due to the geometry of the problem, the quantum well in between nanotubes, a significant portion of the trajectory is such that $q(\tau)||x$. For the significance of time the emitted electron keeps interacting with surrounding TLLs. Our task is then to average out the quantum fluctuations, which can be done for TLL, in order to obtain effective parameters inside $V_{\text{saddle}}(x)$.

In a realistic system, neighboring nanotubes may have a different chirality and parameters, but the tube that is the most metallic, i.e., has the smallest gap, will provide the largest amount of screening. This justifies our approximation of a single-tube dominated process.

Correlation functions in TLL

In Eq. (4) we see that there are two terms in the potential that need to be overcome by the tunneling electron. The first one is due to an interaction between the electron and the hole that has been left behind in the nanodevice and the second one is due to the screened external potential. The question is what is the form of these terms in an environment defined by surrounding 1D nanotubes—TLLs.

In TLL the fermionic correlation functions translate into a bosonic form (here to lighten notation we drop the bosonic field index ν; since bosonic modes are orthogonal, their correlations factorize) which up to a prefactor reads

$$\begin{aligned}&\langle\psi^{\dagger}(x,t)\psi(0,0)\rangle\\&\quad\approx\langle\exp[\phi(x,t)+\theta(x,t)]-[\phi(0,0)+\theta(0,0)]\rangle.\end{aligned}\tag{9}$$

This can be evaluated as a Gaussian integral:

$$\begin{aligned}&\langle\exp\imath A[\phi(x,t)-\phi(0,0)]\rangle\\&\quad=\exp-\tfrac{1}{2}A^2\langle\phi(x,t)\phi(0,0)\rangle=\exp\left(-\tfrac{1}{2}A^2K\ln(r)\right),\end{aligned}\tag{10}$$

where A is some numerical constant and we used the Debye-Waller relation for the average of an exponential. For the dual θ field correlators the procedure is the same; the final result can be recovered by substitution $K\to 1/K$. This leads to power laws with nonuniversal, interaction dependent exponents $\sim K$.

In the example above we have obtained the Green's function for a single particle η (where $A=1/\sqrt{N}$). The probability of electron-hole recombination at (x,t) [after both particles were created at the same point (0,0)] in the simplest approximation will be given by a correlation function of two *distinguishable* copropagating particles (one inside and one on the surface of the nanotube). The entire reasoning goes the same as before, just that in Eq. (9) we need to take two copies of each bosonic field, ultimately producing $A=2/N$. Thus the electron-hole recombination, which is an analog of an image potential, i.e., the last term in Eq. (4), is predicted to have the following scaling:

$$V_{\text{img}}(x)\sim x^{-2^2\eta},\tag{11}$$

with the single particle exponent known to be $\eta=(\sum_{\nu}K_{\nu}+1/K_{\nu})/2N$.

The second term in Eq. (4) is due to an interaction with an external potential that is pulling the electron away from the nanodevice. By itself, the external electric field in the vicinity of the 1D conductor has a very weak spatial dependence, due to an underscreening property of 1D metal, which is known to follow logarithmic dependence $V_0(x)\sim\ln(x)$. The spatial dependence arises then due to extended quantum fluctuations in TLL. Since seminal works by Furusaki [35] it is known that in the limit of the strong potential (in our language work function is equal to or greater than bandwidth) the tunneling process can be described by instanton events which add the following cosine perturbation term to the TLL Hamiltonian:

$$H_{\text{tun}}=F_{\text{ext}}\int dx\,\cos(\theta_{\rho+})\cos(\theta_{\rho-})\cos(\theta_{\sigma+})\cos(\theta_{\sigma-}).$$

Here we took a full fermion tunneling; hence all bosonic fields are involved. The spatial spread of the tunneling amplitude t_{tun}, the probability of these instanton events, is proportional to correlation functions of the canonically conjugate momentum θ_{ν} fields. As the electron moves along the nanotube it will endeavor a series of such tunneling events which can be resummed into the final effective tunneling rate as a geometric series [32]; an accuracy of such approximation has been confirmed by benchmarking with the numerics in our previous work [28]. Thus an overall effect of the quantum fluctuations produces the following spatial dependence $\tilde{t}_{\text{tun}}=F/(1-t_{\text{tun}})$, which for sufficiently large tunneling probability produces the following scaling relation:

$$\tilde{t}_{\text{tun}}\sim x^{2(\sum^{N}1/K_{\nu})/N}.\tag{12}$$

In the presence of an entire array of nanotubes, the electric field that is pulling the carrier is screened—a process described by a dielectric constant: $F_{\text{eff}}=F_{\text{ext}}/\epsilon$. From Dzyaloshinskii-Larkin reasoning we know that inside each TLL the random-phase approximation (RPA) holds and we can also assume that intertube interactions are long range (dilute limit for emitted electrons). Then the dielectric function of the array reads $\epsilon(q)=1+W(q)\chi^{irr}(q)$; thus, for long range electron-electron interactions $W(q)$, in the long-wavelength limit the second term dominates. We take the TLL susceptibility to be an irreducible part of susceptibility and thus upon Fourier transform $\epsilon(x)\approx\chi^{\text{TLL}}(x)$. The static charge susceptibility is proportional to the equal-time correlation function:

$$\chi^{\text{TLL}}(x)=\langle\hat{O}_{\text{CDW}}(x,t=0)\hat{O}_{\text{CDW}}(0,0)\rangle,\tag{13}$$

with

$$\begin{aligned}&\hat{O}_{\text{CDW}}(x,t=0)\\&\quad=\cos[\phi_{\rho+}(x)]\cos[\phi_{\rho-}(x)]\cos[\phi_{\sigma+}(x)]\cos[\phi_{\sigma-}(x)],\end{aligned}\tag{14}$$

so its correlation function scales like $\sim x^{2K}$. The only assumption that we used here is that the action of the external electric

field on the TLL is independent on spin and valley degrees of freedom.

Overall this tunneling due to an external electric field in the vicinity of TLL scales like

$$V_{\text{ext}}(x) \sim \left(x^{\sum_\nu 2/K_\nu} x^{\sum_\nu 2K_\nu}\right)^{1/N_\nu}. \tag{15}$$

We see that both exponents of power laws in Eq. (11) and Eq. (15) have the same absolute value, only the opposite sign. Hence our generalized Fowler-Nordheim formalism applies provided we make the following conjecture:

$$\alpha \to 2\left(\sum_\nu K_\nu + 1/K_\nu\right)\Big/ N_\nu. \tag{16}$$

We can thus explore what the influence is of electron-electron interactions on the tunneling current. To this end we shall use a recently obtained generalization of Fowler-Nordheim theory.

IV. RESULTS: GENERAL CASE

A. Current

The total tunneling current, the quantity that we are interested in, is equal to

$$J(\omega, F) = T(\omega, F) n_{\text{tube}}(\omega, F), \tag{17}$$

where the first term comes from our generalized Fowler-Nordheim theory, Eq. (7), and the second one is a density of states that we shall derive in the following subsection. While $T(\omega)$ determines what is the tunneling probability, the $n_{\text{tube}}(\omega)$ determines how many carriers are there, actually available to tunnel, e.g., when one goes way above the Fermi energy then the tunneling probability will be approaching one (because emitted electrons are above the top of the barrier) but, at the same time, the number of available carriers will go down to zero.

Before we move on to study the effects of $n_{\text{tube}}(\omega, F, x)$ first we present the effect of gFN on $T(\omega)$ in particular including the implications of electron-electron interactions. We assume spin-rotational invariance $K_\sigma = 1$ and for density of states (DOS) we take simply a step function, i.e., Fermi-Dirac distribution at zero temperature in a metal with a constant dispersion. The result is shown in Fig. 2. Indeed we can see that tunneling probability is an increasing function of frequency ω (energy), but the effects of interactions are also important. The growth is fastest for noninteracting carriers $K_\rho = 1$, while the presence of interactions (both repulsive $K_\rho < 1$ and attractive $K_\rho > 1$) smooths the curve. This is a manifestation of the fact that for any $K_\rho \neq 1$ single-particle states fractionalize into collective bosonic states which need to be combined to emit the electron out of the TLL.

Above we assumed a constant density of states along the wire. If this does not hold the formula for the current needs to be generalized:

$$J(\omega, F) = \int dx\, T(\omega, F, x) n_{\text{tube}}(\omega, F, x), \tag{18}$$

where we included the possibility that the tunneling probability may be also dependent on the position, through $x = x_{\text{in}}, x_{\text{out}}$.

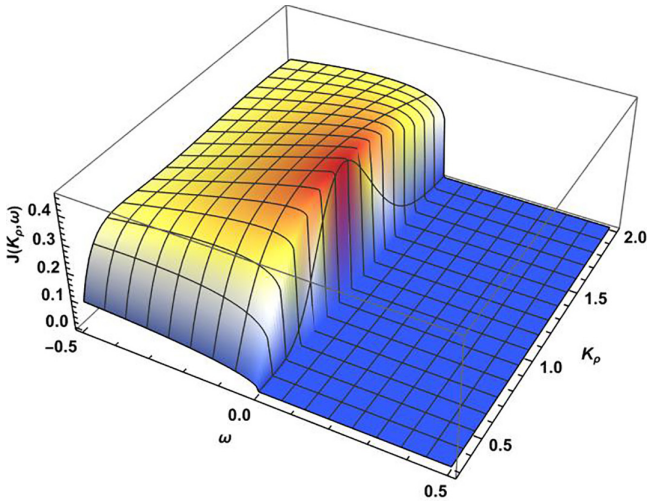

FIG. 2. 3D plots of field emission current $J(K_\rho, \omega)$ as a function of energy ω and TLL charge interaction parameter K_ρ. $J(K_\rho, \omega)$ is plotted for a given constant value of external field $F = 0.8\text{V/m}$ keeping $K_\sigma = 1$.

B. Density of states

The second main ingredient that contributes to the tunneling current is a spectral function of electronic liquid along the nanotube n_{tube}. The DOS encodes the electronic properties of any material, determining its electrical conductivity, thermal conductivity, and optical properties. This is because it provides crucial information about the behavior of electrons, including their occupation and how they propagate. Here we wish to incorporate the effects of interactions since we know that in 1D propagating electrons cannot avoid each other and thus become strongly correlated.

Usually, evaluation of any correlation function in a strongly correlated state is a prohibitively difficult task, let alone finite size and finite temperatures. Calculating spectral function $A(q, \omega)$ for all values of energies in a 1D liquid at $T = 0$ can be done by means of the Bethe ansatz, while for finite temperatures only by means of the most advanced numerical methods such as time-dependent density matrix renormalization group (tDMRG); both results were shown in Ref. [36]. Therein, for the spin chain with characteristic energy J, it was found that a linearized theory works up to energy scales of $\approx 1.5J$. This linearized theory is precisely the TLL framework introduced in the previous section.

Fortunately, as described above, this is possible through the TLL formalism; hence, in the following, we take $n_{\text{tube}}(F, \omega, x) = n_{\text{TLL}}(F, \omega, x)$. The Green's function and thus also DOS for an infinite TLL are well known [37]; actually, we showed the way to obtain it in the previous section. Since in field emission, we are interested in *occupied* states, we shall work with the lesser Green's function.

Thanks to the conformal invariance of the underlying field theory, for infinite 1D wires the TLL correlation functions are known also at finite temperatures. This enables a direct comparison with the experiments that are unavoidably performed at finite temperatures. Remarkably, in Ref. [38], Mattsson and co-workers have obtained finite-temperature LDOS also for a finite size spin-full 1D system. Their result shows explicitly

the LDOS dependence on a distance from the top of the nanotube. Their solution is presented in the Appendix [Eq. (A1)]. We see a product of two $\sinh^{a_i}(x, v_i t)$ functions, each corresponding to a pole of a Green's function characterized by a velocity v_i.

In Ref. [38] the authors used a standard Dirichlet boundary condition that assumes a hard wall boundary at the end of the nanotube, which in turn results in a boundary condition $\phi_v(x = 0) = 0$. However, what is more appropriate for a nanotube in a finite electric field, constantly emitting a stream of electrons, are the radiative boundary conditions as derived in [39]. These are also consistent with a physical situation most likely realized when the residue of metal catalysts rests on each nanotube's top: a small quantum dot in a double tunneling regime is present at the top of the nanotube. Assuming continuity and no voltage drop, between the nanotube and the quantum dot we arrive at the boundary condition for the canonically conjugated field $\theta_{\rho\pm}(x = 0) = cste$. This can be easily accommodated in Mattsson and co-workers' formalism provided that we make a substitution $K_{\rho\pm} \to 1/K_\rho$.

The real space result of Ref. [38] has been written as a product of powers of sine-hyperbolic functions. The difficulty rests in the fact that for our purposes we need frequency dependence of LDOS, which is obtained through partial Fourier transform. Obviously, this can be done through a direct numerical evaluation; however, already in Ref. [38] the singularity of LDOS was pointed out, which needs to be regularized. This is a nontrivial task to achieve for the numerical integration, especially since we wish to use it as a basic ingredient for later calculations. We then turned our attention to possible analytic expressions, for specific cases when the Fourier transform can be done exactly. We have identified a case when an exact analytic solution can be derived. This choice of $-b_c/2 = 1$ and $-b_s/2 = 0$ is the one, for which analytic Fourier transformation is obtained by us (see the Appendixes for the formula). Anticipating results of the further section we state that the case when $-b_c/2 = 1$, $-b_s/2 = 0$ corresponds to $a_c = 2.015$, $a_s = \frac{1}{4}$. This implies $K_{\rho+} = K^* = 0.25$ and we further take $K_{\sigma-} = 1$, which is used in further calculations, while $K_{\rho-}$ and $K_{\sigma+}$ are kept as free parameters. There is only one mode with velocity v_c, the holon, and for this pole, the value b_c automatically determines $K_{\rho+}$. If we had focused on a simple spin-full fermionic chain, then $b_s = 0$ would imply a "noninteracting" [i.e., SU(2) invariant] spin degree of freedom with $K_s = 1$. For the case of the two leg ladder (that we look at in this paper), the other pole has three bosonic modes that contribute, see Eq. (19), and thus even though we set $b_s = 0$ we nevertheless have certain freedom of choice of these TLL parameters. We emphasize that the $b_s = 0$ condition does not mean the complete absence of the spin degree of freedom in the system, as $a_s \neq 0$, but there is no spatial dependence induced by the spin degree of freedom.

Thus our solution works for the physically relevant case when $K_\rho \approx 1/4$ as measured experimentally [40]. This also corresponds to a close vicinity of marginal RG flow for the case of a half-filled band. Proximity of nanotubes to the Mott-insulating phase has been identified in several earlier works [41]. Here we assume that in the charge sector the system can flow towards the Mott phase. The flow would be always towards the critical value $K^* = 1/2$. However, due to weak incommensurability, for instance, due to codoping between single-walled nanotube (SWNT) shells of multi-walled nanotube (MWNT), the system is in a Luther-Emery liquid with the parameter $K^*/2 = 1/4$. If intratube repulsive interactions are too weak to push the system towards these small values, there are always intertube Coulomb interactions that can be incorporated in our modeling and will further modify downwards the $K_{\rho+}$ parameter [31]. This explains why such a value is frequently observed in experiments done on single-walled carbon nanotube (SWCNT). At absolute zero temperature, it is established that DOS diminishes to zero at the Fermi energy following a power law in ω—a so-called zero-bias anomaly. Here we shall analyze the density of states (DOS) for Tomonaga-Luttinger liquids under finite temperature conditions.

Figure 3 illustrates the LDOS as a function of ω and r at various temperatures, where ω is measured relative to the Fermi energy and r is the distance from the boundary. At $\omega = 0$, the energy corresponds to the Fermi level, serving as a critical reference point for energy levels. This dip at $\omega = 0$ is a well-documented signature of 1D physics, known as the "zero-bias anomaly" that has been observed experimentally in various systems, for instance, carbon nanotubes [40] or semiconductor gated wires [42,43] and quite recently even in controlled two-dimensional (2D) to 1D crossover [44]. The figure shows LDOS below and above the Fermi energy, providing valuable insights into the energy distribution characteristics within the confined TLL of the nanotube. We see a profound deep close to $\omega = 0$ and a deep when r is going down to 1. These features are sharper when the temperature is lower; in this case, when $\beta = 200$, it is sharper than when $\beta = 50$. Then, it increases to a maximum when r is a few lattice spacing and then it goes down when we are going deeper into the carbon nanotube. It is important to mention that the double peak structure observed for values where $\omega > 0$ may be probably related to the well-established 1D hallmark known as spin-charge separation that was also experimentally measured in several systems [42,43,45–47].

V. RESULTS FOR NANOTUBES

The results of the previous section can be used to obtain electron emission spectra for arrays of nanotubes. Usually, nanotubes are grown using chemical vapor deposition (CVD) on a prearranged catalyst array and MWNT are obtained. Although a multiwall system is obtained one can always assume that among several ($N > 3$) layers there will be at least one metallic. It is known that a rolled hexagonal lattice, upon perpendicular quantization, may become either a metal or a semiconductor. The first case, realized in approximately one-third of all cases, is described as a two-leg-ladder system that can develop minigaps in some of the bosonic modes. The two legs are present due to two valleys K, K' present in 2D dispersion. This is valid and well established for carbon nanotubes, but not limited to these since any rolled 2D analog based on p orbitals (silicene, stanene, etc.) will share the same general properties albeit with different values of parameters.

The two-leg ladder description is obviously much more complicated than the spin-full chain that we considered so far, as there are four $\rho\pm, \sigma\pm$ instead of two bosonic modes.

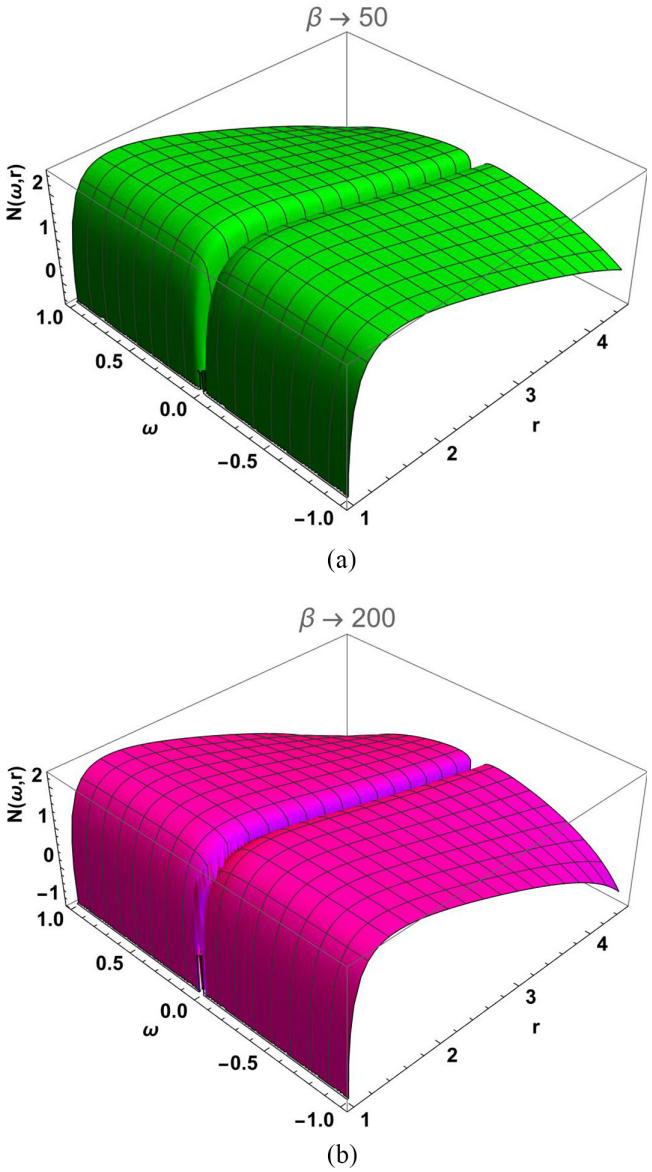

FIG. 3. TLL density of states as a function of energy ω and the distance from the boundary r (tip of the carbon nanotube; unit of r is $1/V_F$), when (a) $\beta = 50$ and (b) $\beta = 200$. The $\beta = \frac{1}{T}$ is inverse temperature with a unit set by the fact that the unit of energy was set by $v_F = 1$.

However, an extremely useful aspect of nanotubes dominated by the long range interaction is that only the velocity of the charge-full $\rho+$ mode, the $v_{\rho+}$, is strongly modified, while for the remaining three modes the respective velocities stay close to V_F. Thanks to the fact that our original formulas for space dependent spectral functions $N(\omega, r)$ can still be applied, however, we need to take into account that now three modes K_ν will contribute to what was before a_s:

$$\tilde{a}_s = \frac{K_{\sigma+}^2 + K_{\sigma+}^{-2} + K_{\sigma-}^2 + K_{\sigma-}^{-2} + K_{\rho-}^2 + K_{\rho-}^{-2}}{8} \tag{19}$$

and

$$\tilde{b}_s = \frac{K_{\sigma+}^2 + K_{\sigma+}^{-2} + K_{\sigma-}^2 + K_{\sigma-}^{-2} + K_{\rho-}^2 + K_{\rho-}^{-2}}{8}. \tag{20}$$

The advantage of this situation is that previously setting $b_s = 0$ determined the value $K_s = 1$, while what we expect now is that, for the case with long-range interactions, three neutral modes with nearly equal velocities $V_{\sigma+} \approx V_{\rho-} \approx V_{\sigma-} = V_F$ contribute to b_s. We see that now, even if we take our specific analytical solution for LDOS, the choice of TLL parameters for the neutral modes is largely arbitrary; thus also the value of α in the tunneling function becomes a free parameter. The most likely situation [48] is that of slow marginal flow due to curvature or spin-orbit driven so-called "dimerization" terms [49] leading towards ultralow temperature ordering of $\cos\phi_{\sigma+}$ and $\cos\phi_{\rho-}$ terms, keeping the σ mode unaffected. Then $K_{\rho-}^{-1} > 1$ will compensate for the effect of $K_{\sigma+} < 1$ and the two together with $K_{\sigma-} \approx 1$ will give at the same time $b_s = 0$ and a nontrivial value for the exponent of correlation function a_s as well as the exponent α inside the tunneling barrier expression. The fact that the two can precisely compensate each other in Ref. [50] was shown to be related to the way SO(6) symmetry is broken, i.e., initially all three neutral modes are degenerated and then assuming a single, valley symmetric perturbation parameter, such as the tubes' curvature, leads to an even deviation of both modes' TLL parameters. It is remarkable that such symmetry can be related to the lack of spatial dependence due to these neutral modes and gives physical meaning to the special Fourier transform solution obtained here by us.

A. Entirely metallic tube

We begin with the simpler case, when the nanotube is entirely metallic, which can happen when an achiral, armchair or zigzag, tube is present among MWNT layers. In this case, all the bosonic modes are massless, because high symmetry prohibits the emergence of any symmetry breaking cosine term (e.g., dimerization) and one can immediately apply the results of the previous section with the substitutions described above.

Figure 4 shows the tunneling current for entirely metallic nanotubes when F is changing from 0.01 to 0.2 V/m. In order to make the case when K_ν parameters do matter, it is best to focus on the small values of F and so we did in this first picture. Here we can clearly see the difference between the different values of $K_{\rho-}$, which means that the values of $K_{\rho-}$ are indeed meaningful quantities. In higher temperature $\beta = 50$, panel (a)] we see a double peak structure, below and above $\omega = 0$; the second one contains both thermal and interaction effects that are entangled. The case $K_{\rho-} = 1$ would correspond to a noninteracting system, the further one is from this value, and the stronger is electron-electron interactions. Thus the difference between red ($K_{\rho-} = 0.85$, weaker interactions) and green ($K_{\rho-} = 0.66$, stronger interactions) allow one to investigate their effect. We see that interactions do increase the amplitude of field emission. Subfigure (b) shows that, for this temperature ($\beta = 200$), there are no thermionic effects and the entire emission is driven by the interactions. For the smaller values of interactions, there is a very tiny emission and for larger interactions the two emission peaks clearly appear.

Figures 5 and 6 illustrate the characteristics of the tunneling current for entirely metallic nanotubes, each described by specific parameters. The metallic nanotubes exhibit

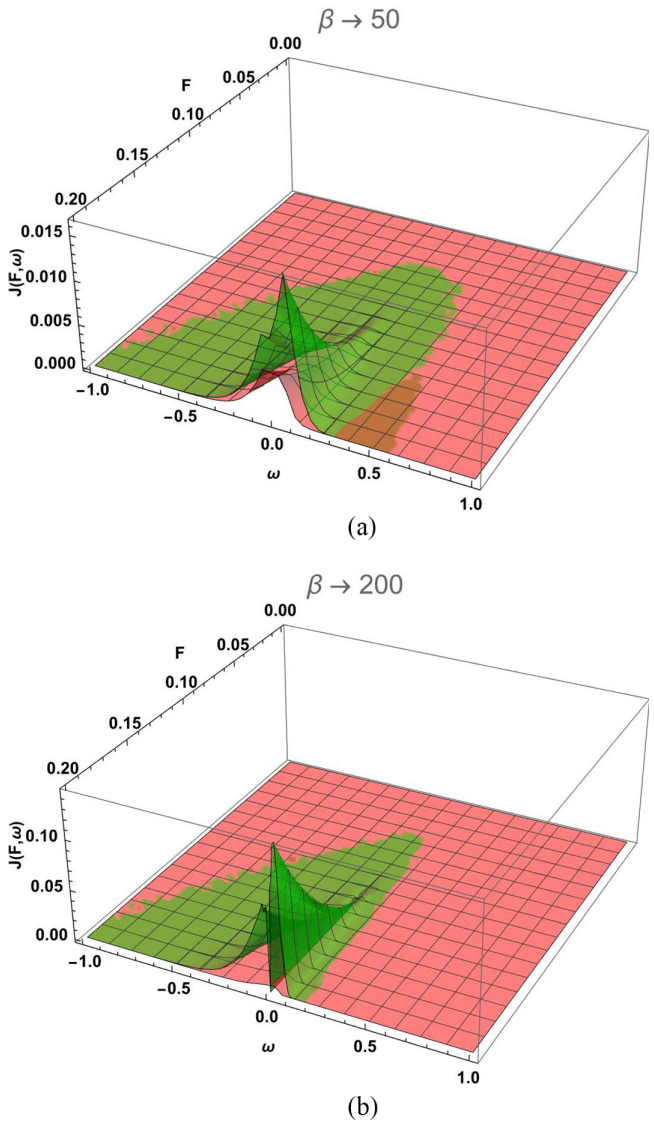

FIG. 4. Tunneling current $J(\omega, F)$ plotted as a function of external electric field F and energy ω measured with respect to Fermi level. The plots are for entirely metallic nanotubes described by the following parameters: (a) $\beta = 50$ and (b) $\beta = 200$; green: $K_{\sigma-} = 1$, $K_{\sigma+} = 1.51$, $K_{\rho-} = 0.66$, and $K_{\rho+} = K^*$; red: $K_{\sigma-} = 1$, $K_{\sigma+} = 1.17$, $K_{\rho-} = 0.85$, and $K_{\rho+} = 0.25$. Here we focus on the lowest values of external electric fields.

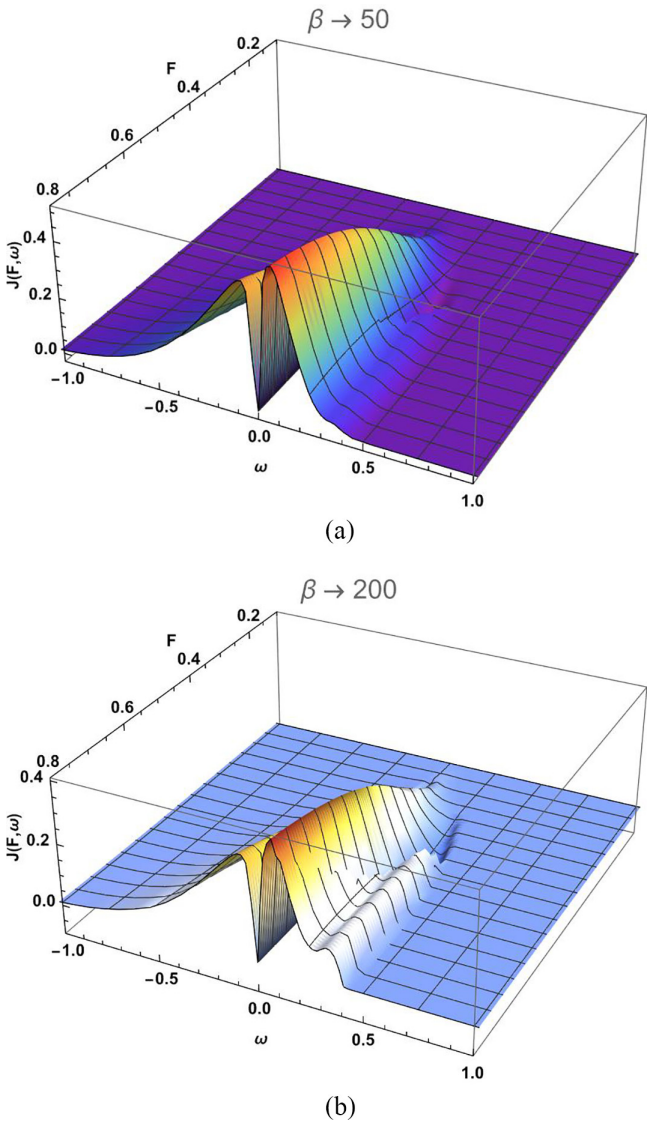

FIG. 5. Tunneling current $J(\omega, F)$ plotted as a function of external electric field F and energy ω measured with respect to Fermi level. The plots are for entirely metallic nanotubes described by the following parameters: $K_{\sigma-} = 1$, $K_{\sigma+} = 1.51$, $K_{\rho-} = 0.66$, and $K_{\rho+} = K^*$, when (a) $\beta = 50$ and (b) $\beta = 200$. The $\beta = 1/T$ is inverse temperature with a unit set by the fact that the unit of energy was set by $v_F = 1$. The color coding follows the J value on the vertical axis.

massless bosonic modes due to their high symmetry that protects against backscattering, resulting in unique electron emission properties. Both figures comprise two subfigures, (a) and (b), corresponding to different values of *temperature*. Subfigure (a) shows the tunneling current as a function of energy and electric field when the temperature is higher $\beta = 50$, while subfigure (b) displays the same for lower temperature $\beta = 200$. In these figures, we see that tunneling current is increasing for negative ω (when ω is changing from -1 to close to 0), the same behavior is visible in Fig. 2 (for the transmission amplitude) and in TLL's LDOS for larger values of x, and hence the peak-like structure for the negative ω appears as a product of both. Next, there is a deep at $\omega = 0$ point, which corresponds to the same feature—the deep visible in TLL's LDOS in Fig. 3. Just like in Fig. 3 the deep is sharper for lower temperatures. When $\omega > 0$ there is a double peak structure, a massive peak, and a smaller shoulder. The shoulder structure is more visible when interactions are stronger $K_{\rho-} = 0.66$ and it is smoother when $K_{\rho-} = 0.85$. When the temperature is higher, the $\omega > 0$ structure has a larger amplitude which is in agreement with an expectation for thermionic emission. Furthermore, all figures show that, as the external electric field F increases, the overall peaks height and area is growing larger. Initially, for lower fields, the height grows fast, but later we observe saturation especially for the thermionic peak ($\omega > 0$). For larger fields we also observe increased range of

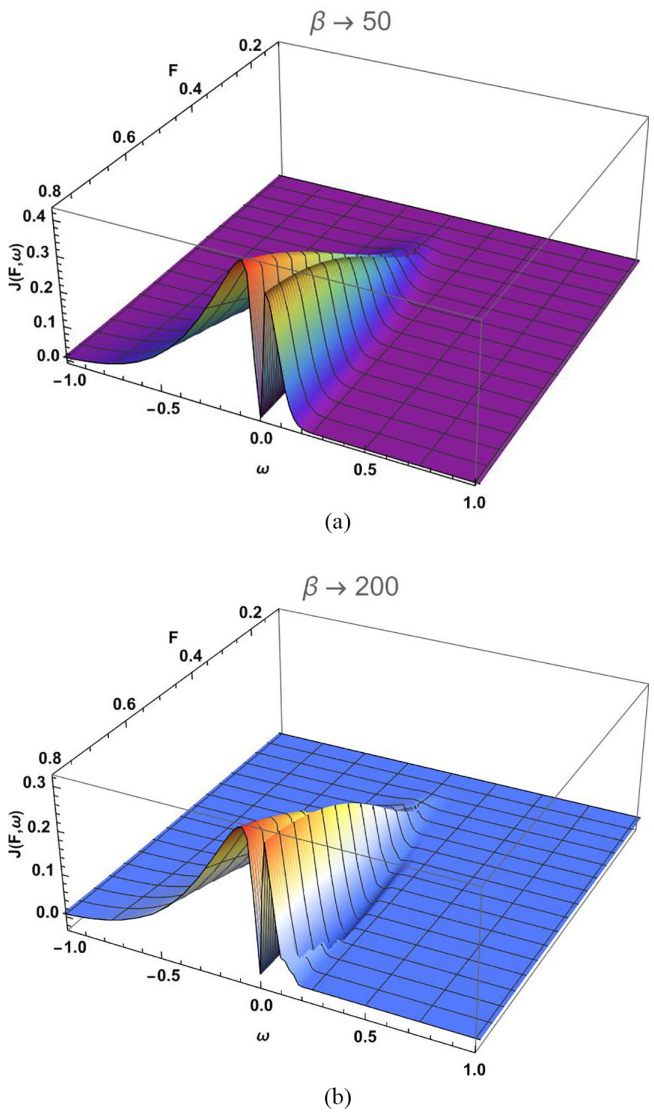

FIG. 6. Tunneling current for entirely metallic nanotubes described by the following parameters: $K_{\sigma-} = 1$, $K_{\sigma+} = 1.17$, $K_{\rho-} = 0.85$, and $K_{\rho+} = K^* = 0.25$, when (a) $\beta = 50$ and (b) $\beta = 200$.

contributing ω and the shoulder feature, which indicates that we are beyond the single particle regime.

B. Case of gapped neutral modes

More complicated, but more likely is the situation that, when the nanotube has lower symmetry, it is chiral, as then the minigaps in some bosonic modes can open. Past research indicates [48] that equal size gaps in $\phi_{\sigma+}$ and $\phi_{\rho-}$ modes are most likely. One needs to add at least the following perturbation to the TLL Hamiltonian:

$$H_{\cos} = g_U \int dx \, \cos(\phi_{\rho-}) \cos(\phi_{\sigma+}), \tag{21}$$

which results in two bosonic fields locking at the minimum of the cosine. By construction the gaps of the two modes are equal and entangled. There are also other cosine terms in a two-leg ladder description, but they contain an equal number of canonically conjugated $\cos\phi_{\sigma-}$ and $\cos\theta_{\sigma-}$ terms,

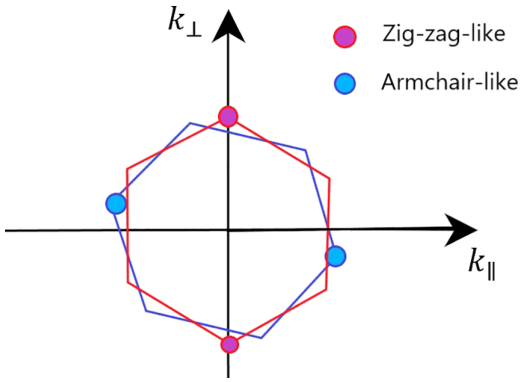

FIG. 7. Perpendicular quantization upon rolling the nanotube. Dots show the position of the Dirac points crossed by the quantized, quasimetallic band. Two cases are possible [51]. Zigzag-like nanotubes: Dirac points collapse to the origin of the longitudinal Brillouin zone, resulting in metallic behavior and armchair-like nanotubes: Dirac points are well separated in longitudinal momentum space, giving rise to metallic behavior.

which implies that an ultrasmall gap is present only through refermionization of this field. We also assumed that the tube is not commensurate; hence umklapp terms, that would involve a $\cos(\phi_{\rho+})$ term, are not present.

What is remarkable is that for the many body problem when the single particle electron emission gap is $\Delta = \Delta_{\sigma+} + \Delta_{\rho-}$ the two-particle probes like charge susceptibility or electron-hole spectral function detect a gap of two times larger size $\Delta_{2p} = 2\Delta$. This implies that for energies $\Delta < \omega < 2\Delta$ we shall have an intermediate regime where the modes $\sigma+$ and $\rho-$ do not contribute to characteristic exponents and certainly do not contribute to characteristic exponent α.

More information about this regime can be gathered from several studies, for instance, by Essler and Tsvelik, where they have computed spectral function for the sine-Gordon model [52,53]. They showed that indeed while the spectral function has a gap Δ below which any tunneling is impossible, the characteristic double dispersion (spinon and holon) of TLL is recovered only for energies above 2Δ. In the intermediate regime, we observe the dispersion characteristic of the gapped state [54,55]. From this we deduce the following *ansatz*: in the intermediate regime we shall take also the a_s exponent inside $N_{\rm TLL}(\omega, r)$ independent of bosonic modes $\sigma+$ and $\rho-$, but also we assume that dielectric properties along the tube are modulated with periodicity q_0, which means that a simple integral for the current $J(\omega)$ is now becoming a Fourier transform:

$$J(\omega, F; T) = \int dr \, \cos(q_0 r) N^{<}_{\rm TLL}(\omega, r) T(\omega, F), \tag{22}$$

where q_0 is the distance between Fermi points, i.e., the distance between the two K, K' valleys measured along the nanotube axis.

The intermediate regime postulated here can be noticed in a two stage activation behavior of $J(\omega, F; T)$ as revealed in the plots below. Depending on the details of the perpendicular quantization condition we can distinguish [51] two types of chiral tubes: zigzag-like and armchair-like; see Fig. 7.

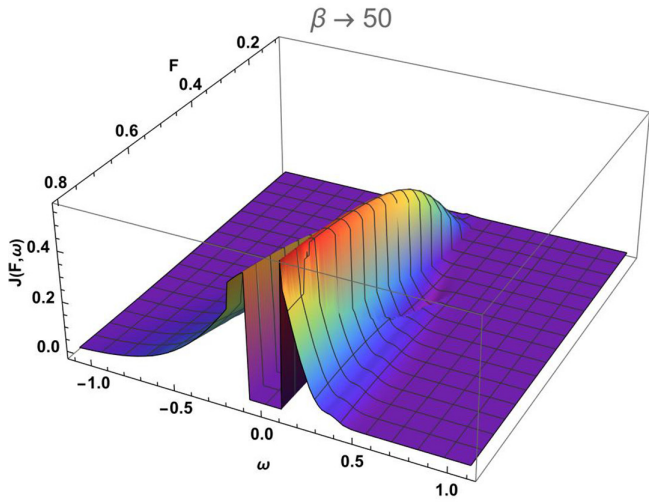

(a)

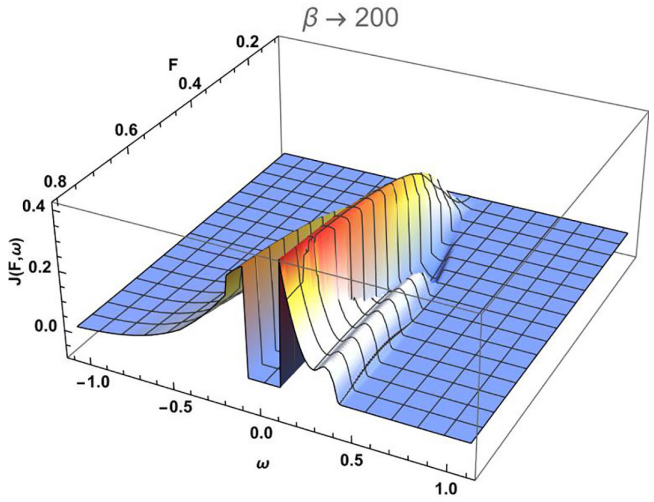

(b)

FIG. 8. Tunneling current for zigzag-like nanotubes described by the following parameters: $K_{\sigma-} = 1$, $K_{\sigma+} = 1.51515$, $K_{\rho-} = 0.66$, and $K_{\rho+} = K^* = 0.25$, when (a) $\beta = 50$ and (b) $\beta = 200$.

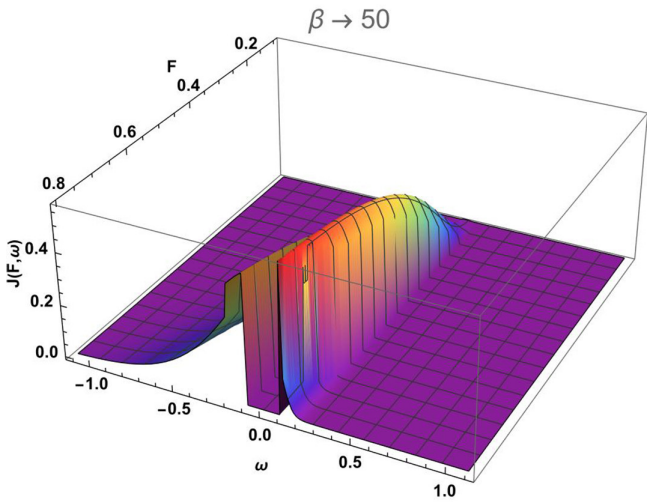

(a)

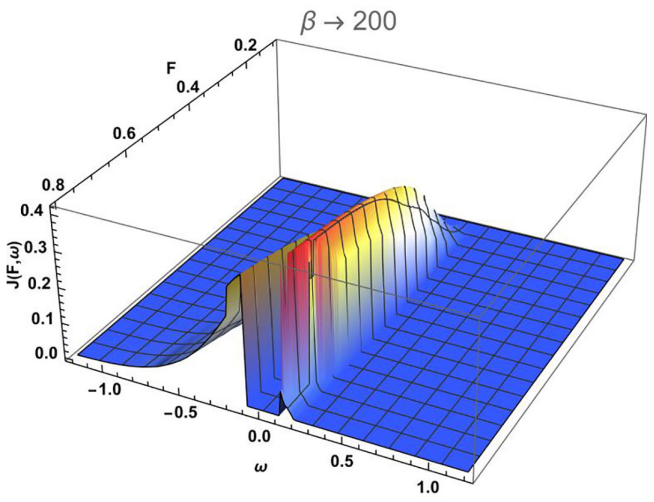

(b)

FIG. 9. Tunneling current for zigzag-like nanotubes described by the following parameters: $K_{\sigma-} = 1$, $K_{\sigma+} = 1.17$, $K_{\rho-} = 0.85$, and $K_{\rho+} = K^* = 0.25$, when (a) $\beta = 50$ and (b) $\beta = 200$.

1. Zigzag-like nanotubes

In this case $q_0 = 0$ and Eq. (22) reduces to the previously used formula, but with a different $N(\omega)$: $N(|\omega| < \omega_0) = 0$ and $N(\omega_0 < |\omega| < 2\omega_0) = N_{2\mathrm{TLL}}(\omega)$, where $N_{2\mathrm{TLL}}(\omega)$ is LDOS for TLL with only two free modes [and the α exponent in $T(\omega)$ modified accordingly]. Figures 8 and 9 present the tunneling current behavior in zigzag-like nanotubes with different interaction parameters. The top and bottom panels in both figures show the tunneling current at different temperatures (a) $\beta = 50$ and (b) $\beta = 200$. Here we choose $\omega_0 = 0.1$. As it is shown in the figures, when $|\omega| < 0.1$, the tunneling current is equal to 0, there is no emission due to the presence of minigaps in some bosonic modes, when $0.2 > |\omega| > 0.1$ there is anomalous tunneling, and when $|\omega| > 0.2$ the behavior of the tunneling current is similar to the previous case (Figs. 5 and 6). In comparison with Figs. 5 and 8, we see differences in the new intermediate regime. The emission peak for $\omega < 0$ now has a larger amplitude and we actually can observe discontinuity at $\omega = -2\omega_0$ that is due to the fact that we have defined $N(\omega)$ in an unphysical, piecewise manner; in reality one expects some crossover between two- and four-mode TLLs (we postpone study of the right crossover function to later study). The larger amplitude of emission is probably due to the fact that two bosonic modes are not mobile; hence they do not need to be captured when a single fermion is reconstituted. The emission peak for $\omega > 0$ is growing faster as a function of F and reaches saturation for smaller values of F. For the largest ω the shoulder peak is even better pronounced especially at lower temperatures and stronger interactions shown in Fig. 5(b).

2. Armchair-like nanotubes

In this case, $q_0 \neq 0$ (actually q_0 can be as large as a third of BZ) and Eq. (22) takes a more complicated Fourier-transform form. In this case, the fact that we know the LDOS distribution along the tube $N^{<}_{\mathrm{TLL}}(\omega, r)$ plays a vital role.

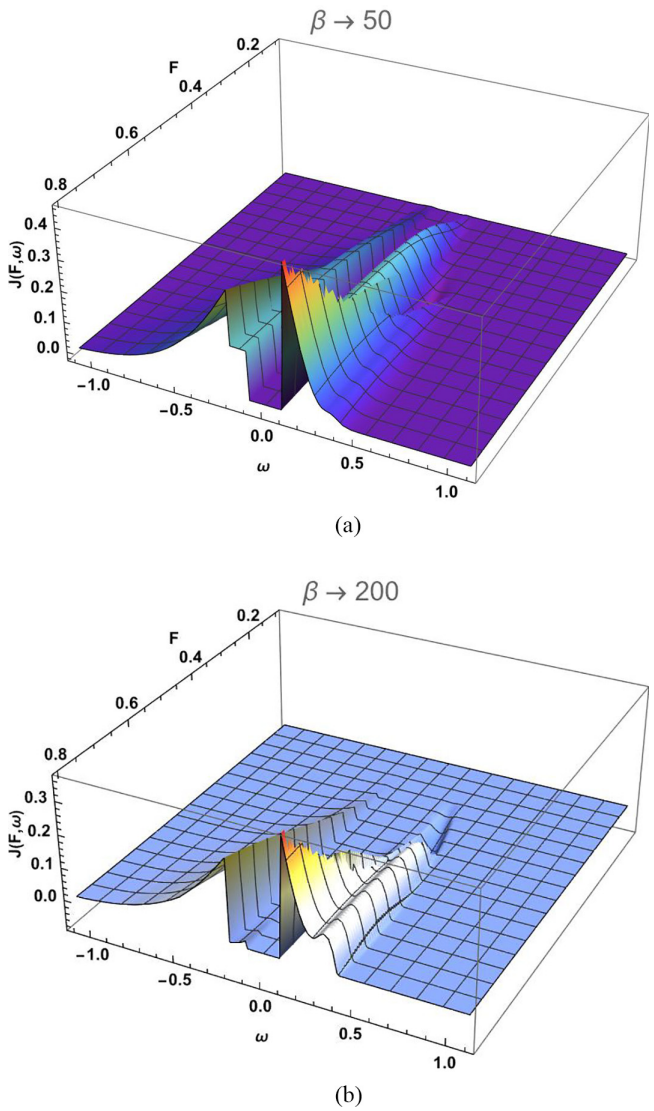

FIG. 10. Tunneling current for armchair-like nanotubes described by the following parameters: $K_{\sigma-} = 1$, $K_{\sigma+} = 1.51$, $K_{\rho-} = 0.66$, and $K_{\rho+} = K^* = 0.25$, when (a) $\beta = 50$ and (b) $\beta = 200$.

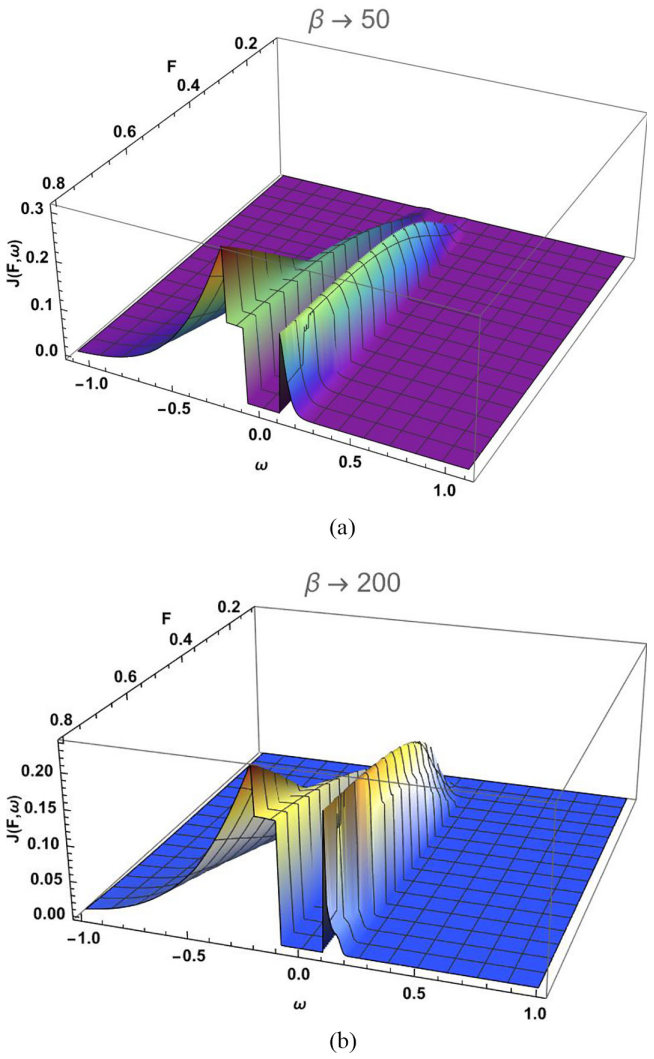

FIG. 11. Tunneling current for armchair-like nanotubes described by the following parameters: $K_{\sigma-} = 1$, $K_{\sigma+} = 1.17$, $K_{\rho-} = 0.85$, and $K_{\rho+} = K^* = 0.25$, when (a) $\beta = 50$ and (b) $\beta = 200$.

Armchair-like nanotubes, unlike zigzag-like nanotubes, exhibit a distinctive behavior: after initial saturation at the same field F like for the zigzag-like tubes [but at a $J(\omega, F)$ amplitude that is two times smaller] we observe that the current starts increasing again at the largest values of F, ultimately reaching the same value of $J(\omega, F)$ like in the zigzag-like tubes. This is due to the periodic potential appearing along the length of the armchair-like nanotubes. This periodicity potentially causes variations in energy landscapes at differing nanotube sections, manifesting as this dual saturation behavior. Figures 10 and 11 present the behavior of the tunneling current in armchair-like nanotubes exhibiting minigaps in bosonic modes, each described by specific parameters. The system is described within the framework of a TLL model. For illustration proposes q_0 is taken equal to $1/(3a)$. Notably, following an initial saturation, a pronounced surge in the current becomes evident. This rapid rise in current can be linked to the periodic potential effects, as these tubes reach a value of $J_{\max} = 0.4$ only after showing further growth at the highest F values. As seen in the figures, when ω is changing from -1 to -0.2, the current gradually increases; then at $\omega = -0.2$ there is a sharp decrease (a discontinuity, like before) and the current stays the same, constant up to the point when $\omega = -0.1$, in the region of ω changing from -0.1 to 0.1 where the current is forced to be 0. At $\omega = 0.1$ there is a sharp increase; in the region of 0.1 to 0.2, it decreases. When $\omega > 0.2$, the current behaves as in the previous case (Figs. 8 and 9). We can now compare this with results for zigzag-like tubes, namely Figs. 8 and 9 and Figs. 10 and 11, respectively. We see that now, in the periodically modulated case, the increase of $J(F)$ is actually delayed; for the case of stronger interactions an intense growth is present only for the largest electric fields F and no saturation is observed. The amplitudes of all current peaks are smaller, as clearly revealed by the discontinuity at $\omega = -0.2$. The presence of spatial modulation of the nanotube properties should be thus visible, in this nontrivial way, in the (ω, F) characteristics of the material.

VI. DISCUSSION AND CONCLUSIONS

The main outcome of this work is to show that the effects of emission due to temperature and electron-electron interactions can be simultaneously and nonperturbatively taken into account in a closed analytic formula. We see that both lead to potentially observable effects. Since in our work we set the bandwidth as a unit of energy, the results are easily transferable from one material to another, for instance from carbon to silicon nanotubes. An open issue is the role of many-body interactions when the emission takes place from the tip of the nanotube. There were studies showing an emergence of additional purely many-body peaks on the tip [55] showing that a standard single-particle approach may be after all insufficient also here. This will obviously depend on the microscopic structure of the tip in a given system; we leave an in-depth study of this effect for the future.

While the focus of this study is mainly on the linear regime of low energy, there have been significant advances in the field that tackle the nonlinear regime in carbon nanotubes. Notably, recent works in Refs. [56] and [57] have explored nonlinear Luttinger liquids in carbon nanotubes, giving deeper layers of insight into these systems. Such advancements provide exciting prospects for future study. In principle it is possible to include curvature as a momentum/frequency dependent velocity $V_F(q)$ (which holds for the neutral modes' part of LDOS); however, what remains to be established is how the holon velocity v_ρ and TLL parameters K_ν would be affected by this change of the model and what momentum dependence they would acquire. Thus extending our model to incorporate these nonlinear effects is highly nontrivial and has to be left as an intriguing direction for future research. Curvature is equivalent to a mass term in the Hamiltonian and there were experimental efforts to measure how this mass changes upon 1D to 2D crossover [44]. In the context of arrays of nanotubes that would be a case when electrons start to hybridize in between the tubes, i.e., the intertube distance of an angstrom scale, that is also beyond the scope of this work and actually beyond arrays that have been synthesized so far.

The UV cutoff within the Tomonaga-Luttinger liquid theory in our approach is purely phenomenological, i.e., we assume that at some energy scale the linear approximation of the spectrum will not be applicable any longer. For SWCNT this can be related to the inverse lattice spacing, but for MWCNT the characteristic length scale may be much longer. Recent theoretical and experimental advances have provided a more detailed understanding of it. Works such as [58,59] have provided a deeper theoretical understanding, while experimental studies [60] have substantiated these observations.

Moreover, while discussing experimental techniques, it is essential to differentiate between angle-resolved photoemission spectroscopy (ARPES) [61] and the FE method (which is the focus of our study). In FE, the focus is on varying the amplitude of the external electric field, adjusting frequency through photon-assisted FE, or regulating back-gate potential. In ARPES, which has also been done in CNTs [62], we need to resolve problems of light wave interference and light polarization (that determine dipole moments of the transition)—everything under the assumption that the amplitude of the dynamic external field is weak (within a linear response regime). Though the two techniques differ in their foundational principles, they complement each other, as seen in the emergent research on photon assisted FE [63].

However, taking into account the geometrical smallness of the tip, Coulomb-blockade effects should be always present. This will in general decrease the current from the tip, thus increasing the importance of the side-surface (background) current studied here.

Another open issue is the experimental relevance of the observed phenomena. Naturally, the temperature and the external field are parameters that can be varied in an experiment; our formula offers a possibility to fit these characteristics. Importantly, the TLL parameters can be also modified by experimental means. For instance, the ways the $K_{\sigma+}$ can be affected by an external magnetic field have been studied in detail in the work of Egger *et al.* [64]. This parameter will be also modified for nanotubes made out of heavier elements, with stronger spin-orbit coupling. On the other hand, the $K_{\rho-}$ parameter depends on the strength of the effective on-site Hubbard parameter and on the strength of intervalley hybridization. Both of these are largely unknown and can also lead to a minigap in the spectrum whose effects we have been investigated in the later part of this study.

This last remark, about unknown parameters in effective low-energy physics of multiwall nanotubes, brings up another relevant aspect of our work. In our plots we see clear, qualitative differences between various types of nanotubes. These can be even quantified if the TLL parameters are sought after. This implies that our results may serve as a tool to *diagnose* arrays of MWNT in order to determine, through low energy field emission, what fraction of nanotubes represents what properties and also whether the fabrication method has any influence on that. Although more crude, this may be a fast and efficient alternative for Raman spectroscopy methods [65] that are used now for this daunting task of distinguishing chirality of nanotubes. It is worth emphasizing that the field mission can also be used with microscopically small electrodes. We should thus be able to obtain valuable space resolved information about the many-body effects in arrays of nanotubes.

Our study will also have implications for the modeling of nanotube arrays. Although we are focused on one specific range of parameters, where our analytic formula works, the advantage of our result is that it is an exact method with no approximation involved. Thus it can serve as a benchmark for numerical calculations. The fact that it is analytic means that the formula may be easily transferred from one material to the other, simply by modifying parameters. It can be also applied for processes other than FE, where electron tunneling in a large side surface of nanotube arrays plays a vital role, for instance, in chemical and materials engineering processes geared towards catalysis or hydrogen storage.

ACKNOWLEDGEMENT

Authors acknowledge financial support of EU through MSCA (Grant No. 847639).

APPENDIX A: FOURIER TRANSFORM OF LDOS

The finite temperature, real space (and real time) LDOS in a 1D TLL has been obtained in Ref. [38]. In the following

Mattsson, Eggert, and Johanesson have given the expression for frequency (energy) dependent LDOS as a regularized integral (which they solved numerically):

$$N(\omega,\beta,r)=\frac{2}{\alpha\pi^2}v_c^{-a_c}v_s^{-a_s}\int_0^\infty dt\ \cos\gamma(t)\Bigg[\cos\omega t\left(\frac{\sinh\frac{\pi}{\beta}t}{\frac{\pi}{\beta}\alpha}\right)^{-a_s-a_c}\left|\frac{\sinh\frac{\pi}{v_c\beta}(2r+v_ct)\sinh\frac{\pi}{v_c\beta}(2r-v_ct)}{\sinh^2\frac{2\pi r}{v_c\beta}}\right|^{-b_c/2}$$
$$\times\left|\frac{\sinh\frac{\pi}{v_s\beta}(2r+v_st)\sinh\frac{\pi}{v_s\beta}(2r-v_st)}{\sinh^2\frac{2\pi r}{v_s\beta}}\right|^{-b_s/2}-\left(\frac{t}{\alpha}\right)^{-a_s-a_c}\left|1-\left(\frac{v_ct}{2r}\right)^2\right|^{-b_c/2}\left|1-\left(\frac{v_st}{2r}\right)^2\right|^{-b_s/2}\Bigg],\tag{A1}$$

where the exponents for space-independent $a_{s,c}=\frac{K_{s,c}{}^2+K_{s,c}^{-2}}{4}$ and space-dependent $b_{s,c}=\frac{K_{s,c}^{-2}-K_{s,c}{}^2}{4}$ parts depend on TLL parameters. In the past work [38] the two-modes TLL is considered and hence the dependence only on charge and spin parameters $K_{s,c}$, with boundary condition set on $\cos\phi_{c,s}$ fields (hence only $K_{s,c}$ not $1/K_{s,c}$ enter their expression).

Here we have found that in a special case $-b_c/2=1$ and $-b_s/2=0$ the integral can be performed analytically, and the resulting indefinite integral reads

$$N(\omega,\beta,r)=\frac{2}{\alpha\pi^2}v_c^{-a_c}v_s^{-a_s}\Bigg[\pi^{a_c+a_s}\operatorname{csch}^2\left(\frac{2\pi r}{v_c\beta}\right)\Bigg(2^{-2+a_c+a_s}e^{-\frac{\pi t(a_c+a_s)}{\beta}}\left(-e^{-\frac{\pi t}{\beta}}+e^{\frac{\pi t}{\beta}}\right)^{-a_c-a_s}\left(-1+e^{\frac{2\pi t}{\beta}}\right)\cosh\left(\frac{4\pi r}{\beta v_c}\right)$$
$$\times\sinh^{a_c+a_s}\left(\frac{\pi t}{\beta}\right)\left(\frac{\beta\sinh\left(\frac{\pi t}{\beta}\right)}{\alpha}\right)^{-a_c-a_s}\left(\frac{e^{\frac{t(-i\beta\omega+\pi a_c+\pi a_s)}{\beta}}\beta\,{}_2F_1\left[1,\frac{1}{2}\left(2-\frac{i\beta\omega}{\pi}-a_c-a_s\right),\frac{1}{2}\left(2-\frac{i\beta\omega}{\pi}+a_c+a_s\right),e^{\frac{2\pi t}{\beta}}\right]}{i\beta\omega-\pi a_c-\pi a_s}\right.$$
$$\left.-\frac{e^{\frac{t(i\beta\omega+\pi a_c+\pi a_s)}{\beta}}\beta\,{}_2F_1\left[1,\frac{1}{2}\left(2+\frac{i\beta\omega}{\pi}-a_c-a_s\right),\frac{1}{2}\left(2+\frac{i\beta\omega}{\pi}+a_c+a_s\right),e^{\frac{2\pi t}{\beta}}\right]}{i\beta\omega+\pi a_c+\pi a_s}\right)$$
$$-2^{-3+a_c+a_s}e^{-\frac{\pi t(a_c+a_s)}{\beta}}\left(-e^{-\frac{\pi t}{\beta}}+e^{\frac{\pi t}{\beta}}\right)^{-a_c-a_s}\left(-1+e^{\frac{2\pi t}{\beta}}\right)\beta\sinh^{a_c+a_s}\left(\frac{\pi t}{\beta}\right)\left(\frac{\beta\sinh\left(\frac{\pi t}{\beta}\right)}{\alpha}\right)^{-a_c-a_s}$$
$$\times\left(-\frac{e^{\frac{t(-2\pi-i\beta\omega+\pi a_c+\pi a_s)}{\beta}}\,{}_2F_1\left[1,-\frac{1}{2}\left(\frac{i\beta\omega}{\pi}+a_c+a_s\right),\frac{1}{2}\left(-\frac{i\beta\omega}{\pi}+a_c+a_s\right),e^{\frac{2\pi t}{\beta}}\right]}{-2\pi-i\beta\omega+\pi a_c+\pi a_s}\right.$$
$$-\frac{e^{\frac{t(2\pi-i\beta\omega+\pi a_c+\pi a_s)}{\beta}}\,{}_2F_1\left[1,\frac{1}{2}\left(4-\frac{i\beta\omega}{\pi}-a_c-a_s\right),\frac{1}{2}\left(4-\frac{i\beta\omega}{\pi}+a_c+a_s\right),e^{\frac{2\pi t}{\beta}}\right]}{2\pi-i\beta\omega+\pi a_c+\pi a_s}$$
$$-\frac{e^{\frac{t(-2\pi+i\beta\omega+\pi a_c+\pi a_s)}{\beta}}\,{}_2F_1\left[1,\frac{1}{2}\left(-\frac{i\beta\omega}{\pi}+a_c+a_s\right),\frac{1}{2}\left(\frac{i\beta\omega}{\pi}+a_c+a_s\right),e^{\frac{2\pi t}{\beta}}\right]}{-2\pi+i\beta\omega+\pi a_c+\pi a_s}$$
$$\left.-\frac{e^{\frac{t(2\pi+i\beta\omega+\pi a_c+\pi a_s)}{\beta}}\,{}_2F_1\left[1,\frac{1}{2}\left(4+\frac{i\beta\omega}{\pi}-a_c-a_s\right),\frac{1}{2}\left(4+\frac{i\beta\omega}{\pi}+a_c+a_s\right),e^{\frac{2\pi t}{\beta}}\right]}{2\pi+i\beta\omega+\pi a_c+\pi a_s}\right)\Bigg)$$
$$-\frac{1}{4}t\left(\frac{t}{\alpha}\right)^{-a_c-a_s}\left(\frac{t^2v_c^2}{r^2(a_c+a_s-3)}-\frac{4}{a_c+a_s-1}\right)\Bigg],\tag{A2}$$

where ${}_2F_1()$ is a Gauss hypergeometric function. The Fourier transform of the second ($T=0$) part of Eq. (A1) is simply a power law and had been known before; it serves to regularize the singularity of the first term.

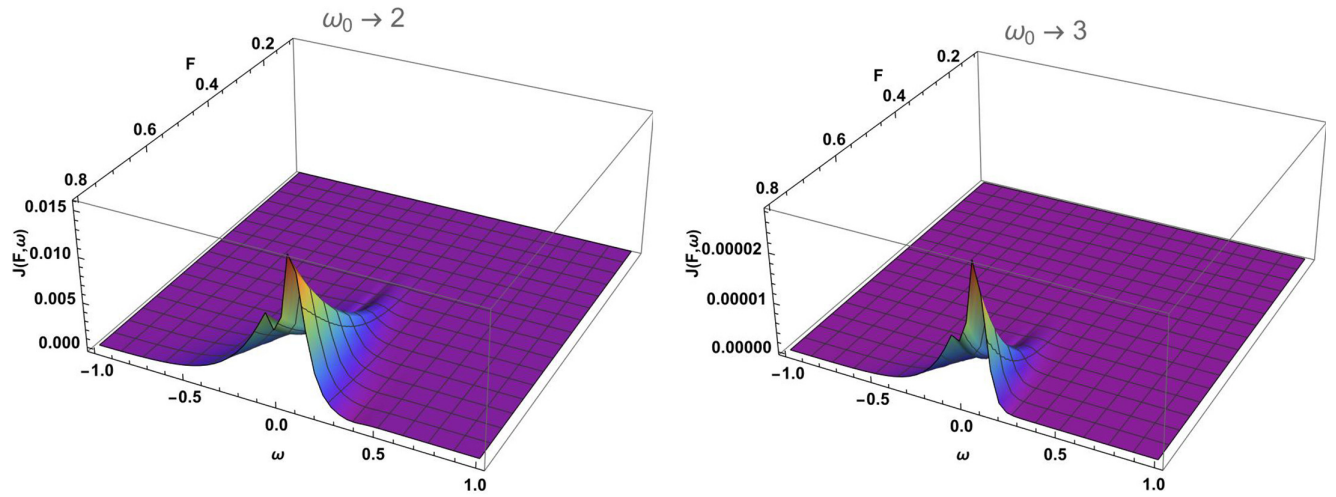

(a) (b)

FIG. 12. Tunneling current for nanotubes described by the following parameters: $K_{\sigma-} = 1$, $K_{\sigma+} = 1.17$, $K_{\rho-} = 0.66$, $K_{\rho+} = K^* = 0.25$, and $\beta = 50$, when (a) $\omega_0 = 2$ and (b) $\omega_0 = 3$.

APPENDIX B: CHEMICAL POTENTIAL VARIATION

1D metal can screen the external electric field only partially; hence we can expect a finite slope of chemical potential when the nanotube is subjected to a strong external electric field. The problem of a chemical potential ν in a TLL under external bias has been solved in [39]. Since in our case, by taking $K_{\rho+} \approx 1/4$, we deal with TLL in a vicinity of Mott transition we extend that result by considering continuous distribution of unitary scattering centers, λ_B, in the notation of that paper. We can then use the exact analytical solution obtained therein, or to be precise a derivative of it:

$$F = \mathrm{Im}\left[\psi\left(0.5 + \frac{0.5 + \imath(2U_x - 1.5F)}{2\pi T}\right)\right], \tag{B1}$$

where we associated the four-voltage potential derivative with an external electric field to which the nanotube is subjected. A solution of this equation U_x is the desired slope of electrochemical potential, a quantity that we include inside our formulas.

APPENDIX C: DEPENDENCE ON WORK FUNCTION

Our formalism also enables us to directly modify the work function of the material under consideration. We inspect this additional feature here.

Figures 12 and 13 present the tunneling current in the case of different work functions. Figure 12 is also compared with Fig. 5(a) and Fig. 13 is compared with 5(b), where $\omega_0 = 1$. As it is shown in the figures when we have a higher work function the tunneling current is smaller, as the barrier that the election has to overcome to go out is becoming much larger.

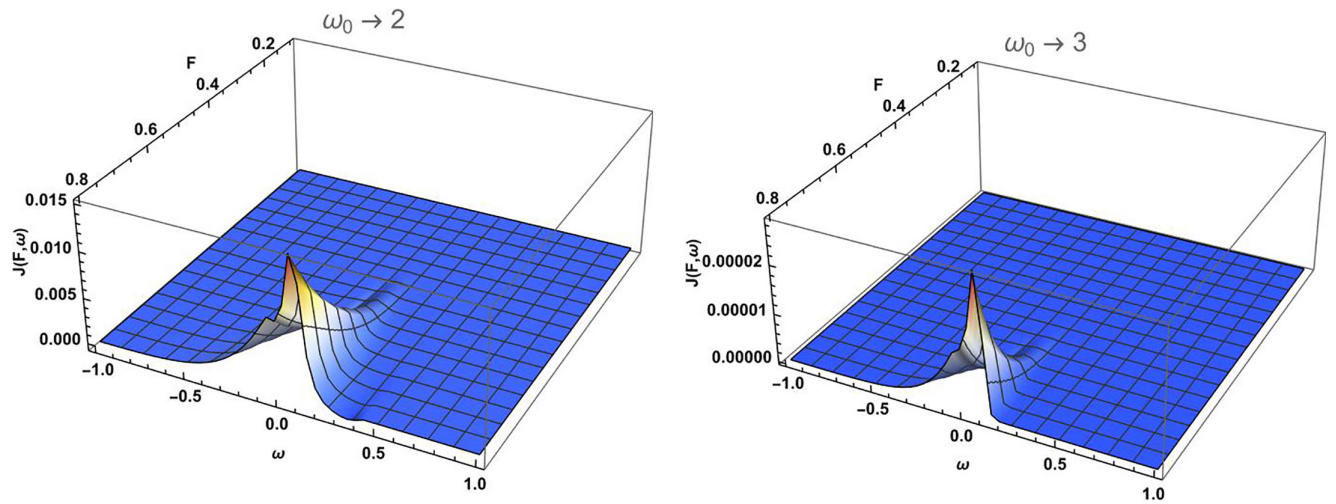

(a) (b)

FIG. 13. Tunneling current for nanotubes described by the following parameters: $K_{\sigma-} = 1$, $K_{\sigma+} = 1.17$, $K_{\rho-} = 0.66$, $K_{\rho+} = K^* = 0.25$, and $\beta = 200$, when (a) $\omega_0 = 2$ and (b) $\omega_0 = 3$.

[1] C. W. Johnson, A. K. Schmid, M. Mankos, R. Röpke, N. Kerker, E. K. Wong, D. F. Ogletree, A. M. Minor, and A. Stibor, Near-monochromatic tuneable cryogenic niobium electron field emitter, Phys. Rev. Lett. **129**, 244802 (2022).

[2] D. B. Williams and C. B. Carter, *Transmission Electron Microscopy: A Textbook for Materials Science* (Springer, Berlin, 2009).

[3] V. E. Cosslett, *Practical Electron Microscopy* (Butterworths Scientific Publications, London, 1951).

[4] W. Zhu, *Vacuum Microelectronics* (John Wiley & Sons, New York, 2001).

[5] G. N. Fursey, Field emission in vacuum micro-electronics, Appl. Surf. Sci. **215**, 113 (2003).

[6] V. Filip, L. D. Filip, and H. Wong, Review on peculiar issues of field emission in vacuum nanoelectronic devices, Solid-State Electron. **138**, 3 (2017).

[7] R. H. Fowler and L. Nordheim, Electron emission in intense electric fields, Proc. R. Soc. London A **119**, 173 (1928).

[8] V. T. Binh, S. T. Purcell, N. Garcia, and J. Doglioni, Field-emission electron spectroscopy of single-atom tips, Phys. Rev. Lett. **69**, 2527 (1992).

[9] D. L. Jaeger, J. J. Hren, and V. V. Zhirnov, Local electrostatic effects of surface structure on field emission, J. Appl. Phys. **93**, 691 (2003).

[10] A. Kyritsakis, G. C. Kokkorakis, J. P. Xanthakis, T. L. Kirk, and D. Pescia, Self focusing of field emitted electrons at an ellipsoidal tip, Appl. Phys. Lett. **97**, 023104 (2010).

[11] A. Mayer, A comparative study of the electron transmission through one-dimensional barriers relevant to field-emission problems, J. Phys.: Condens. Matter **22**, 175007 (2010).

[12] K. L. Jensen, D. Finkenstadt, A. Shabaev, S. G. Lambrakos, N. A. Moody, J. J. Petillo, H. Yamaguchi, and F. Liu, A photoemission moments model using density functional and transfer matrix methods applied to coating layers on surfaces: Theory, J. Appl. Phys. **123**, 045301 (2018).

[13] C. Wang, L. Qiao, C. Qu, W. Zheng, and Q. Jiang, First-principles calculations on the emission properties of pristine and n-doped carbon nanotubes, J. Phys. Chem. C **113**, 812 (2009).

[14] Z. Zheng, X. Zhang, Z. Zhang, R. Tan, J. Zhao, Q. Li, and H. Qin, Observation of high thermionic field emission current density from spun carbon fibers fabricated from multiwall carbon nanotubes, J. Mater. Sci.: Mater. Electron. **26**, 1234 (2015).

[15] J.-M. Bonard, H. Kind, T. Stöckli, and L.-O. Nilsson, Field emission from carbon nanotubes: The first five years, Solid-State Electron. **45**, 893 (2001).

[16] Q. H. Wang, A. A. Setlur, J. M. Lauerhaas, J. Y. Dai, E. W. Seelig, and R. P. H. Chang, A nanotube-based field-emission flat panel display, Appl. Phys. Lett. **72**, 2912 (1998).

[17] S. Fan, M. G. Chapline, N. R. Franklin, T. W. Tombler, A. M. Cassell, and H. Dai, Self-oriented regular arrays of carbon nanotubes and their field emission properties, Science **283**, 512 (1999).

[18] A. O. Gogolin and A. Komnik, Field emission from Luttinger liquids and single-wall carbon nanotubes, Phys. Rev. Lett. **87**, 256806 (2001).

[19] A. Komnik and A. O. Gogolin, Multiparticle effects in nonequilibrium electron tunneling and field emission, Phys. Rev. B **66**, 035407 (2002).

[20] K. L. Jensen, *Field Emission - Fundamental Theory to Usage* (John Wiley & Sons, Ltd, New York, 2014), pp. 1–29.

[21] V. N. Popov, Carbon nanotubes: properties and application, Mater. Sci. Eng., R **43**, 61 (2004).

[22] M. S. Dresselhaus, G. Dresselhaus, P. C. Eklund, and A. M. Rao, Carbon nanotubes, in *The Physics of Fullerene-Based and Fullerene-Related Materials* (Springer, Berlin, 2000), pp. 331–379.

[23] C. Kim, Y. S. Choi, S. M. Lee, J. T. Park, B. Kim, and Y. H. Lee, The effect of gas adsorption on the field emission mechanism of carbon nanotubes, J. Am. Chem. Soc. **124**, 9906 (2002).

[24] A. Goodsell, T. Ristroph, J. A. Golovchenko, and L. V. Hau, Field ionization of cold atoms near the wall of a single carbon nanotube, Phys. Rev. Lett. **104**, 133002 (2010).

[25] S.-D. Liang and L. Chen, Generalized Fowler-Nordheim theory of field emission of carbon nanotubes, Phys. Rev. Lett. **101**, 027602 (2008).

[26] E. L. Murphy and R. H. Good, Thermionic emission, field emission, and the transition region, Phys. Rev. **102**, 1464 (1956).

[27] J. H. B. Deane and R. G. Forbes, The formal derivation of an exact series expansion for the principal Schottky-Nordheim barrier function v, using the gauss hypergeometric differential equation, J. Phys. A: Math. Theor. **41**, 395301 (2008).

[28] N. Grigoryan, A. Roszkiewicz, and P. Chudzinski, Generalizing Fowler-Nordheim tunneling theory for an arbitrary power law barrier, Phys. Status Solidi B **260**, 2200599 (2023).

[29] R. G. Forbes, Use of a spreadsheet for fowler–nordheim equation calculations, J. Vac. Sci. Technol. B **17**, 534 (1999).

[30] R. G. Forbes and J. H. B. Deane, Reformulation of the standard theory of Fowler–Nordheim tunnelling and cold field electron emission, Proc. R. Soc. A **463**, 2907 (2007).

[31] H. J. Schulz, Long-range coulomb interactions in quasi-one-dimensional conductors, J. Phys. C **16**, 6769 (1983).

[32] T. Saso, Y. Suzumura, and H. Fukuyama, Localization and interaction in one-dimensional electron systems, Prog. Theor. Phys. Suppl. **84**, 269 (1985).

[33] T. L. Schmidt and A. Komnik, On the visibility of electron-electron interaction effects in field emission spectra, Solid State Commun. **135**, 455 (2005).

[34] S. Coleman, Fate of the false vacuum: Semiclassical theory, Phys. Rev. D **15**, 2929 (1977).

[35] A. Furusaki and N. Nagaosa, Single-barrier problem and anderson localization in a one-dimensional interacting electron system, Phys. Rev. B **47**, 4631 (1993).

[36] B. Lake, D. A. Tennant, J.-S. Caux, T. Barthel, U. Schollwöck, S. E. Nagler, and C. D. Frost, Multispinon continua at zero and finite temperature in a near-ideal Heisenberg chain, Phys. Rev. Lett. **111**, 137205 (2013).

[37] T. Giamarchi, *Quantum Physics in One Dimension* (Clarendon Press, Oxford, 2003), Vol. 121.

[38] A. E. Mattsson, S. Eggert, and H. Johannesson, Properties of a Luttinger liquid with boundaries at finite temperature and size, Phys. Rev. B **56**, 15615 (1997).

[39] R. Egger and H. Grabert, Applying voltage sources to a Luttinger liquid with arbitrary transmission, Phys. Rev. B **58**, 10761 (1998).

[40] M. Bockrath, D. H. Cobden, J. Lu, A. G. Rinzler, R. E. Smalley, L. Balents, and P. L. McEuen, Luttinger-liquid behaviour in carbon nanotubes, Nature (London) **397**, 598 (1999).

[41] V. V. Deshpande, B. Chandra, R. Caldwell, D. S. Novikov, J. Hone, and M. Bockrath, Mott insulating state in ultraclean carbon nanotubes, Science **323**, 106 (2009).

[42] O. M. Auslaender, H. Steinberg, A. Yacoby, Y. Tserkovnyak, B. I. Halperin, K. W. Baldwin, L. N. Pfeiffer, and K. W. West, Spin-charge separation and localization in one dimension, Science **308**, 88 (2005).

[43] Y. Jompol, C. J. B. Ford, J. P. Griffiths, I. Farrer, G. A. C. Jones, D. Anderson, D. A. Ritchie, T. W. Silk, and A. J. Schofield, Probing spin-charge separation in a tomonaga-luttinger liquid, Science **325**, 597 (2009).

[44] P. M. T. Vianez, Y. Jin, W. K. Tan, Q. Liu, J. P. Griffiths, I. Farrer, D. A. Ritchie, O. Tsyplyatyev, and C. J. B. Ford, Decoupling of the many-body effects from the electron mass in GaAs by means of reduced dimensionality, Phys. Rev. B **107**, 115128 (2023).

[45] B. J. Kim, H. Koh, E. Rotenberg, S.-J. Oh, H. Eisaki, N. Motoyama, S.-i. Uchida, T. Tohyama, S. Maekawa, Z.-X. Shen *et al.*, Distinct spinon and holon dispersions in photoemission spectral functions from one-dimensional $SrCuO_2$, Nat. Phys. **2**, 397 (2006).

[46] R. Claessen, M. Sing, U. Schwingenschlögl, P. Blaha, M. Dressel, and C. S. Jacobsen, Spectroscopic signatures of spin-charge separation in the quasi-one-dimensional organic conductor TTF-TCNQ, Phys. Rev. Lett. **88**, 096402 (2002).

[47] J. Vijayan, P. Sompet, G. Salomon, J. Koepsell, S. Hirthe, A. Bohrdt, F. Grusdt, I. Bloch, and C. Gross, Time-resolved observation of spin-charge deconfinement in fermionic Hubbard chains, Science **367**, 186 (2020).

[48] P. Chudzinski, Spin-orbit coupling and proximity effects in metallic carbon nanotubes, Phys. Rev. B **92**, 115147 (2015).

[49] S. T. Carr, A. O. Gogolin, and A. A. Nersesyan, Interaction induced dimerization in zigzag single wall carbon nanotubes, Phys. Rev. B **76**, 245121 (2007).

[50] D. Controzzi and A. M. Tsvelik, Excitation spectrum of doped two-leg ladders: A field theory analysis, Phys. Rev. B **72**, 035110 (2005).

[51] M. Marganska, P. Chudzinski, and M. Grifoni, The two classes of low-energy spectra in finite carbon nanotubes, Phys. Rev. B **92**, 075433 (2015).

[52] F. H. L. Essler and A. M. Tsvelik, Weakly coupled one-dimensional Mott insulators, Phys. Rev. B **65**, 115117 (2002).

[53] F. H. L. Essler, A. M. Tsvelik, and G. Delfino, Quasi-one-dimensional spin-1/2 Heisenberg magnets in their ordered phase: Correlation functions, Phys. Rev. B **56**, 11001 (1997).

[54] Mathematically, this is related to the fact that the energy and momentum are given by cosh and sinh function of rapidity q and we recover the simple linear relation of TLL only when $q > 2$, i.e., when $\tanh q \to 1$.

[55] D. F. Urban and A. Komnik, Interaction-induced beats of Friedel oscillations in quantum wires, Phys. Rev. Lett. **100**, 146602 (2008).

[56] S. Wang, S. Zhao, Z. Shi, F. Wu, Z. Zhao, L. Jiang, K. Watanabe, T. Taniguchi, A. Zettl, C. Zhou *et al.*, Nonlinear Luttinger liquid plasmons in semiconducting single-walled carbon nanotubes, Nat. Mater. **19**, 986 (2020).

[57] P. M. T. Vianez, Y. Jin, M. Moreno, A. S. Anirban, A. Anthore, W. K. Tan, J. P. Griffiths, I. Farrer, D. A. Ritchie, A. J. Schofield *et al.*, Observing separate spin and charge fermi seas in a strongly correlated one-dimensional conductor, Sci. Adv. **8**, eabm2781 (2022).

[58] A. Imambekov, T. L. Schmidt, and L. I. Glazman, One-dimensional quantum liquids: Beyond the Luttinger liquid paradigm, Rev. Mod. Phys. **84**, 1253 (2012).

[59] O. Tsyplyatyev, A. J. Schofield, Y. Jin, M. Moreno, W. K. Tan, C. J. B. Ford, J. P. Griffiths, I. Farrer, G. A. C. Jones, and D. A. Ritchie, Hierarchy of modes in an interacting one-dimensional system, Phys. Rev. Lett. **114**, 196401 (2015).

[60] Y. Jin, O. Tsyplyatyev, M. Moreno, A. Anthore, W. K. Tan, J. P. Griffiths, I. Farrer, D. A. Ritchie, L. I. Glazman, A. J. Schofield *et al.*, Momentum-dependent power law measured in an interacting quantum wire beyond the luttinger limit, Nat. Commun. **10**, 2821 (2019).

[61] S. Borisenko, 99 years of ARPES, Nat. Rev. Phys. **3**, 539 (2021).

[62] M. S. Dresselhaus, R. E. Smalley, G. Dresselhaus, and P. Avouris, Electron spectroscopy studies of carbon nanotubes, *Carbon Nanotubes: Synthesis, Structure, Properties, and Applications*, Topics in Applied Physics (Springer, Berlin, Heidelberg, 2003), pp. 247–272.

[63] R. Haindl, K. Köster, J. H. Gaida, M. Franz, A. Feist, and C. Ropers, Femtosecond tunable-wavelength photoassisted cold field emission, Appl. Phys. B **129**, 40 (2023).

[64] A. Schulz, A. De Martino, and R. Egger, Spin-orbit coupling and spectral function of interacting electrons in carbon nanotubes, Phys. Rev. B **82**, 033407 (2010).

[65] J. Maultzsch, S. Reich, and C. Thomsen, Chirality-selective Raman scattering of the *D* mode in carbon nanotubes, Phys. Rev. B **64**, 121407(R) (2001).